Chapter 2

Electrohydrodynamic instabilities in nematics

CHAPTER 2

ELECTROHYDRODYNAMIC INSTABILITIES IN NEMATICS

2.1 INTRODUCTION

Hydrodynamic instabilities in isotropic liquids are well known [1]. The classic example is the Rayleigh-Benard instability in thin liquid layers subjected to an adverse temperature gradient. Above a critical value of the temperature gradient the system becomes unstable and breaks up into a set of convective rolls whose size and shape depend on the details of the boundary conditions. Similar instabilities are also found in nematics [2]. In addition they also exhibit convective instabilities under the action of an external electric field [2-4]. These electroconvective or electrohydrodynamic (EHD) instabilities were first observed in the 1930's [5]. However, a detailed study of these were taken up only in the 60's after the technological importance of the electro-optic properties of nematics was recognized. Most of the studies have been on materials with negative or weakly positive dielectric anisotropy and positive conductivity anisotropy The mechanism for the EHD instabilities in these materials is now well understood. A major part of the work reported in this thesis is on this class of nematics. Hence the relevant experimental and theoretical studies on EHD instabilities in these materials is summarized below.

2.2 WILLIAMS DOMAIN INSTABILITY

The Williams domain instability is observed in homogeneously aligned thin layers of a nematic with negative or weakly positive dielectric anisotropy (ϵ_a) and positive conductivity anisotropy (σ_a), under the action of an external DC or low-frequency AC electric field. It was independently discovered by Williams [6] and Zvereva and Kapustin [7]. A typical experimental set up to study this instability is shown in Fig.1. A thin layer of a nematic is sandwiched between two transparent conducting glass plates with the director parallel to them. The thickness of the layer is usually of the order of tens of micrometres. When a sufficiently large electric field is applied between the two glass plates the medium gives rise to an optical pattern consisting of a set of bright striations called Williams domains (Fig.2). If the field is increased further, the system becomes turbulent and scatters light strongly. This is called the dynamic scattering mode [8].

There have been a large number of experimental investigations on the Williams domain instability [3,9,10]. The important facts established by these studies are summarized below.

-The instability is observed under DC and low-frequency AC

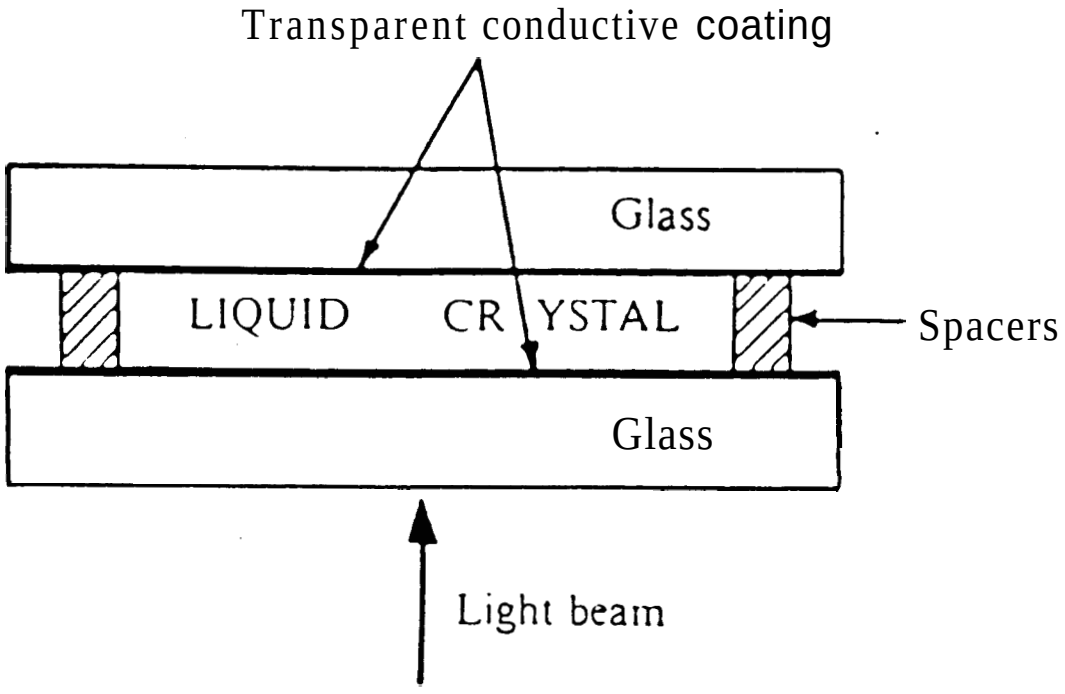

Fig.1. Experimental arrangement for observing Williams domains.

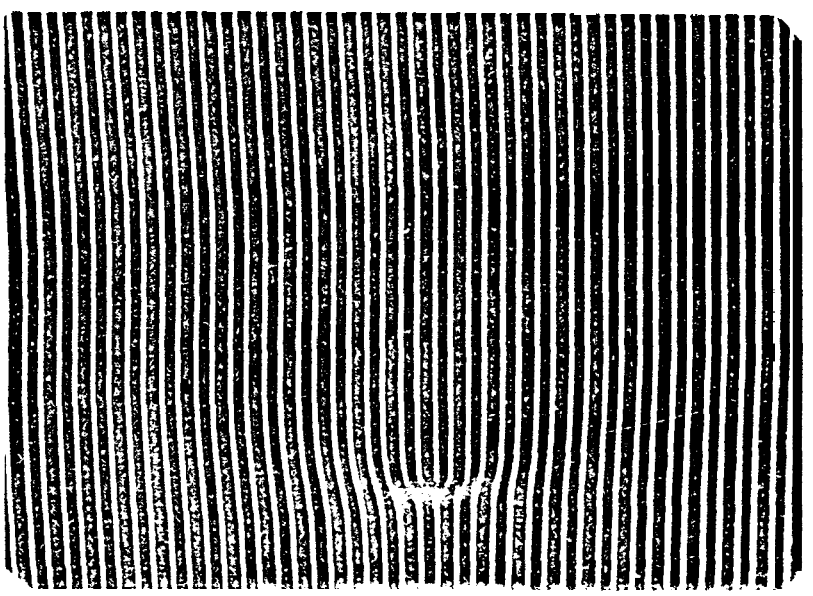

Fig.2. Williams domains observed in MBBA. (7.5 V, 64 Hz). (from Ref.3).

electric fields.

- It is characterized by a threshold voltage, ie, the voltage at which the system becomes unstable is independent of the thickness of the sample.
- The width of the domains is approximately equal to the thickness of the sample.
- When viewed in linearly polarized light, the optical pattern disappears if the plane of polarization is normal to $\hat{n}_{,,}$ the initial orientation of the director, indicating that the distortion of the director field is confined to the plane containing $\hat{n}_o$ and $\vec{E}$.
- The appearance of the domain pattern is accompanied by the onset of cellular flow in the medium. Observations on the motion of tracer particles clearly show that adjacent cells have opposite vorticity.
- Two sets of optical patterns are seen, one above and the other below the plane of the sample.

The situation can be schematically illustrated as shown in Fig.3. At the onset of the instability the medium breaks up into a set of hydrodynamic rolls. Because of the coupling between flow and the orientation of the director, this steady flow leads to a static periodic distortion of the director field. Since the material is birefringent the sample now behaves like an array of alternating convex and concave cylindrical lenses, creating a set of real

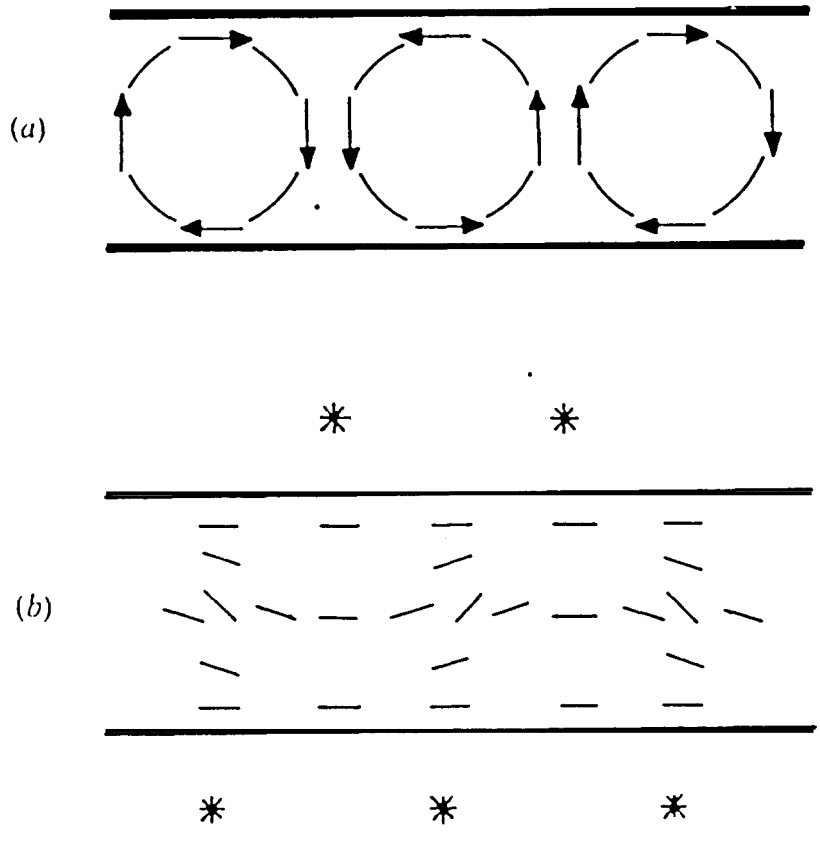

Fig.3. (a) Flow and (b) director orientation patterns in Williams domains. The periodic orientation pattern and the consequent refractive index variation gives rise to the bright domain lines (indicated by the stars) above and below the sample. (from Ref.10).

images of the light source above and a set of virtual images below the plane of the sample.

In appearance the Williams domain instability is very similar to the Rayleigh-Benard instability with two-dimensional rolls. However, while the direction of the rolls in the latter case is determined by the boundary conditions, in the former case, it is determined by the initial orientation of the director which acts as an internal constraint.

2.3 THE CARR - HELFRICH MECHANISM

A mechanism for the Williams domain instability was proposed by Helfrich [11] based on the suggestion by Carr [12] that the conductivity anisotropy could lead to the formation of space charges in a nematic with a suitable type of deformation of the director field.

Consider an infinitesimal bend fluctuation of the director field in a homogeneously aligned nematic layer with a negative dielectric anisotropy subjected to a DC electric field $\vec{E}$ (Fig.4). The current carriers in a nematic are the impurity ions and since $\sigma_{\parallel} > a$, it is easier for the ions to move along the director than normal to it. As a result space charges are formed in the medium,

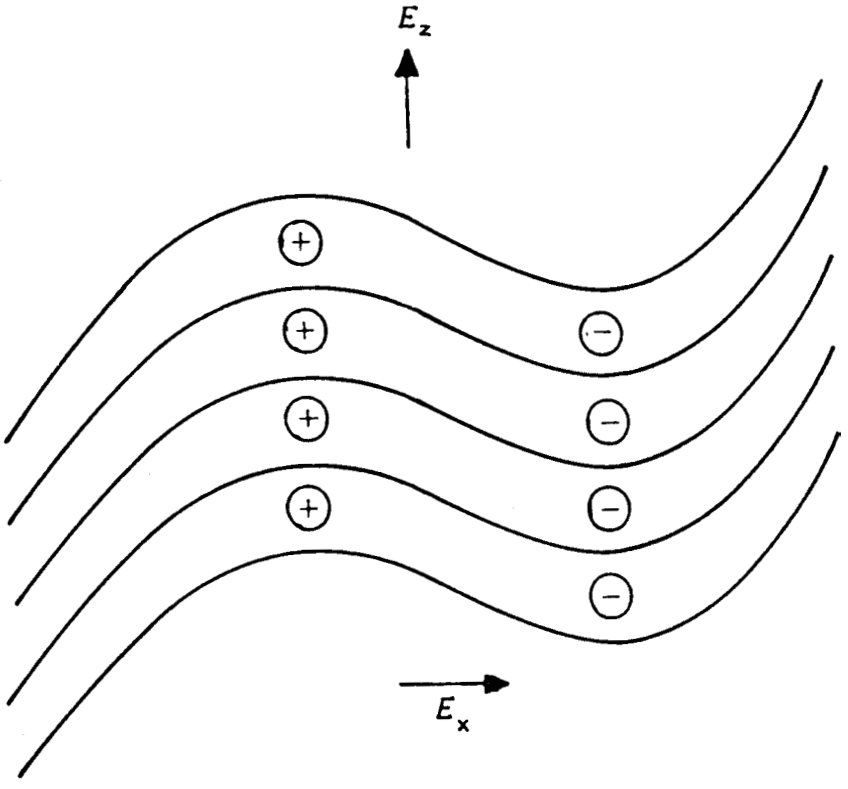

Fig.4. Space charge formation in an applied electric field E_z caused by a bend fluctuation of the director in a nematic with positive conductivity anisotropy. The resulting transverse field is E_x. (from Ref.11).

which in turn give rise to an internal electric field normal to the applied field $\vec{E}$. The force on the space charges due to $\vec{E}$ tends to set them in motion creating a macroscopic flow when the field is sufficiently large. While the dielectric torque on the director due to is stabilizing, the hydrodynamic torque due to the flow and the dielectric torque due to the internal electric field are both destabilizing. Hence if $\vec{E}$ is sufficiently large, an infinitesimal bend distortion of the director field gets amplified and the system becomes unstable and breaks up into hydrodynamic cells. The cellular flow leads to a static periodic distortion of the director field and gives rise to the optical domain pattern. A linear stability analysis of the DC EHD instability in nematics based on the above mechanism was worked out by Helfrich [11] and it is discussed below.

The Helfrich Model

Consider a nematic layer of thickness d, lying in the XY plane and subjected to a DC electric field $\vec{E}_a$ along Z (Fig.4). Let the director $\hat{n}_o$ in the unperturbed state be along the X-axis. The medium is assumed to be infinite in extent in the XY plane so that the lateral boundary conditions are neglected. Consider a bend fluctuation of the director field with $\hat{n}$ in the XZ plane, making a small

angle 8 with the X-axis. This creates a space charge density Q in the medium. The action of E_a on Q in turn gives rise to a flow in the medium, described by the velocity field $\vec{v}$, above the threshold of the instability. In this model the boundary conditions at the two surfaces of the nematic layer are neglected and hence the variables in the problem depend only on X. Further, because of this simplification, only the Z-component of the velocity appears in the equations describing the system. Retaining only the linear terms, the director in the distorted state is given by $\hat{n}=(1,0,\theta)$. The system is described by the following equations.

1) The Poisson equation

$$\mathrm{div}\vec{D} = 4\pi Q,$$

where $\vec{D}$ is the displacement vector. Substituting for $\vec{D}$ (see Eq.6, chapter 1) we get

$$\epsilon_{\parallel} (dE_x/dX) + \epsilon_a E_a(d\theta/dX) = 4 \pi Q \qquad (1)$$

where E_x is the transverse field in the medium due to the space charge formation.

2) The charge conservation equation

$$(\partial Q/\partial t) + \mathrm{div}\, \vec{J} = 0 ,$$

where $\vec{J}$ is the current density. The time dependence can be neglected as we are considering stationary convection

under DC excitation. Using Eq.8, Chapter 1, We get

$$a_{,,}\ (dE_x/dX) + \sigma_a E_a (d\theta/dX) = 0 \qquad (2)$$

3) the equation of motion [13]

$$\rho(d\vec{v}/dt) + \text{div}\ (\rho \vec{v}\vec{v}) = \text{div}\ (\bar{\bar{\sigma}} + \bar{\bar{\sigma}}') + Q\vec{E}\ ,$$

where $\bar{\bar{\sigma}}$ and $\bar{\bar{\sigma}}'$ are the elastic and viscous torques respectively. Confining our attention to stationary solutions and retaining only the linear terms the following equation is obtained

$$-\eta\ (d^2v_z/dX^2) = Q E_a \qquad (3)$$

where $\eta = \frac{1}{2}(a_4 + a_5 - a_2)$.

4) The torque balance equation

$$\vec{\Gamma}^{hy} = \vec{\Gamma}^{d} + \vec{\Gamma}^{\epsilon}\ ,$$

where the three terms represent the torque exerted by the director on the flow, the elastic torque and the dielectric torque due to the total electric field on the director, respectively. This leads to

$$K_3\ (d^2\theta/dX^2) + \epsilon_a \sigma_\perp E_a^2\ \theta\ /(4\pi\ \sigma_{||}) - a_2(dv_z/dX) = 0 \qquad (4)$$

Eliminating E_x , v_z and Q in terms of θ from Eqs.1-4, we get

$$K_3 (d^2\theta/dX^2) - [\alpha_2 \epsilon_\parallel /(4\pi\eta)](\sigma_a/\sigma_\parallel - \epsilon_a/\epsilon_\parallel) E_a^2 \theta + [\epsilon_a \sigma_\perp /(4\pi \sigma_\parallel)] E_a^2 \theta = 0 \qquad (5)$$

In this model the rolls are assumed to be formed with their wavevector along $\hat{n}_o$. Taking $\theta = \theta_o \cos(q X)$, we get

$$E_a^2 = 4 \pi q^2 K_3 /[\epsilon_a \sigma_\perp/\sigma_\parallel - \alpha_2 \epsilon_\parallel (\sigma_a/\sigma_\parallel - \epsilon_a/\epsilon_\parallel)/\eta] \qquad (6)$$

This expression gives the threshold field of the instability as a function of the wave vector of the distortion. As the above analysis does not take into account the boundary conditions it cannot predict the value of q that the system exhibits at the threshold. Since the distortion energy is larger for larger q while the dissipation due to the transverse flow is larger for smaller q, we can assume that the width of the domains must be comparable to the thickness of the nematic layer. Putting $q = \pi/d$, d being the thickness, we get a voltage threshold given by

$$V_{th}^2 = 4 \pi^3 K_3 /[\epsilon_a \sigma_\perp /\sigma_\parallel - \alpha_2 \epsilon_\parallel (\sigma_a/\sigma_\parallel - \epsilon_a/\epsilon_\parallel)/\eta] \qquad (7)$$

This expresion is found to be in qualitative agreement with the experiments [3].

Calculations Including The Boundary Conditions

An extension of the Helfrich model including the boundary conditions was developed by Penz and Ford [14] and Pikin [15]. The treatment of Ref.14 is discussed below. The analysis now becomes two dimensional with all the variables depending both on X and Z. In addition to the Z-component there is also an X-component of the velocity. Assumming the medium to be incompressible these two are related by the continuity equation div $\vec{v} = 0$.

Taking solutions of the form

$\theta = \theta_o \exp(i\vec{q}.\vec{r})$, $E_x = E_o \exp(i\vec{q}.\vec{r})$,
$v_z = v_o \exp(i\vec{q}.\vec{r})$, $v_x = -S\, v_o \exp(i\vec{q}.\vec{r})$,
and $p = p_o \exp(i\vec{q}.\vec{r})$, where $S = q_z/q_x$,

for the variables, the system is described by the following equations.

1) The charge conservation equation,

$$[\sigma_\perp S^2 + \sigma_{||}]\, E_o + \sigma_a E_a \theta_o = 0 \qquad (8)$$

2) The X-component of the equation of motion

$$p_o + i[S^2 q_z \eta_2 + q_z \eta_3]\, v_o = 0 \qquad (9)$$

where $\eta_2 = \frac{1}{2}(a_3 + a_4 + a_6)$ and $\eta_3 = \frac{1}{2}(a_3 + a_4 + 2a_5 + a_6)$.

3) The Z-component of the equation of motion

$$-iq_z p_o + [\eta_4 q_z^2 - \eta_1 q_x^2]\, v_o + (iE_a/4\pi)(\epsilon_\perp S\, q_z + \epsilon_{\parallel}\, q_x)E_o + [i\epsilon_a q_x/4\pi]\, E_a^2 \theta_o = 0 \qquad (10)$$

where, $\eta_1 = \frac{1}{2}(a_4 + a_5 - a_2)$ and $\eta_4 = \frac{1}{2}(a_2 - a_4 + a_5)$.

4) The Y-component of the torque balance equation

$$i(a_2 q_x - a_3 S\, q_z)\, v_o + [K_3 q_x^2 + K_1 q_z^2 - (\epsilon_a/4\pi)\, E_a^2]\, \theta_o - (\epsilon_a/4\pi)\, E_a E_o = 0 \qquad (11)$$

Equations 8-11 are a set of linear homogeneous equations in the amplitudes p_o, v_o, E_o and θ_o. For the existence of non-trivial solutions the determinant of the coefficients should vanish. This condition leads to the following relation between S and E_a/q_x.

$$(1 + S^2)[(a_2 - S^2 a_3)(\sigma_\perp \epsilon_{\parallel} - \sigma_{\parallel} \epsilon_\perp)\, E_a^2/(4\pi q_x^2) - (\eta_1 + S^2 \eta_2)\{(K_3 + K_1 S^2)(\sigma_{\parallel} + S^2 \sigma_\perp) - \epsilon_a \sigma_\perp (1 + S^2)\, E_a^2/(4\pi q_x^2)\}] = 0 \qquad (12)$$

Eq.(12) is a fourth order algebraic equation in S^2. Therefore the 8 roots S_j come in $\pm$ pairs. There are also 8 boundary conditions to be satisfied at the electrodes.

$$\theta\ (Z=\pm d/2) = 0,\ E_x\ (Z=\pm d/2) = 0,$$

$$v_x\ (Z=\pm d/2) = 0,\ v_z\ (Z=\pm d/2) = 0.$$

The boundary condition on 8 leads to the equation

$$\sum_j \theta_j \exp(iS_j\delta) \exp(iq_x X) = 0,$$

where θ_j are arbitrary coefficients to be determined by the boundary condition and $\delta = q_x d/2$. The other boundary conditions also lead to similar equations. Thus we obtain a set of linear homogeneous equations and the boundary value determinant (BVD) associated with these equations must be zero for a solution to exist. The symmetry of the boundary conditions at Z=±d/2 and the symmetry of the S values coming in ± pairs allows a reduction of the set of 8 equations to two independent sets of 4 equations. The BVD will vanish if either of the two 4x4 determinants is zero. One of the two determinants is reproduced below.

$$D_{ij} = 0\ , \qquad i,j = 1,4 \tag{13}$$

The elements of the determinant are:

$D_{1j} = \cos(S_j\delta)$, $D_{2j} = S_j \sin(S_j\delta)$, $D_{3j} = M_j D_{1j}$ and $D_{4j} = N_j D_{3j}$.

where $N_j = (\sigma_\perp S_j^2 + \sigma_{||})/\sigma_\perp$ and

$$M_j = (1 - S_j^2 a_3/a_2)/[(S_j^2 + K_3/K_1)(S_j^2 + \sigma_{||}/\sigma_\perp) - E_a^2 \epsilon_a (1 + S_j^2)/(4\pi K_1 q_x^2)].$$

The other determinant is obtained by interchanging sines and cosines in the one given above.

Eqs.(12) and (13) together form a characteristic value problem. The calculations are made numerically for a given set of values of the material parameters. Choosing the applied voltage V_a and 6, the roots S_j of Eq. (12) are first found. These are then substituted in the BVD and its value is determined. In general the BVD will not be zero for an arbitrary choice of V_a and δ. Keeping V_a fixed a new value of 6 is chosen and the process is repeated till the BVD becomes zero. The calculations are then repeated for a different value of V_a . The lowest value of V_a satisfying Eqs.(12) and (13) is the threshold voltage and the corresponding value of 6 gives the wavevector of the rolls at the onset of the instabi1ity. V_a as a function of 6 obtained using the material parameters of MBBA is shown Fig.5. The threshold voltage is found to be about 6 volts in good agreement with experiments. Further, the width of the domains at the threshold, obtained from the calculations is comparable to the sample thickness.

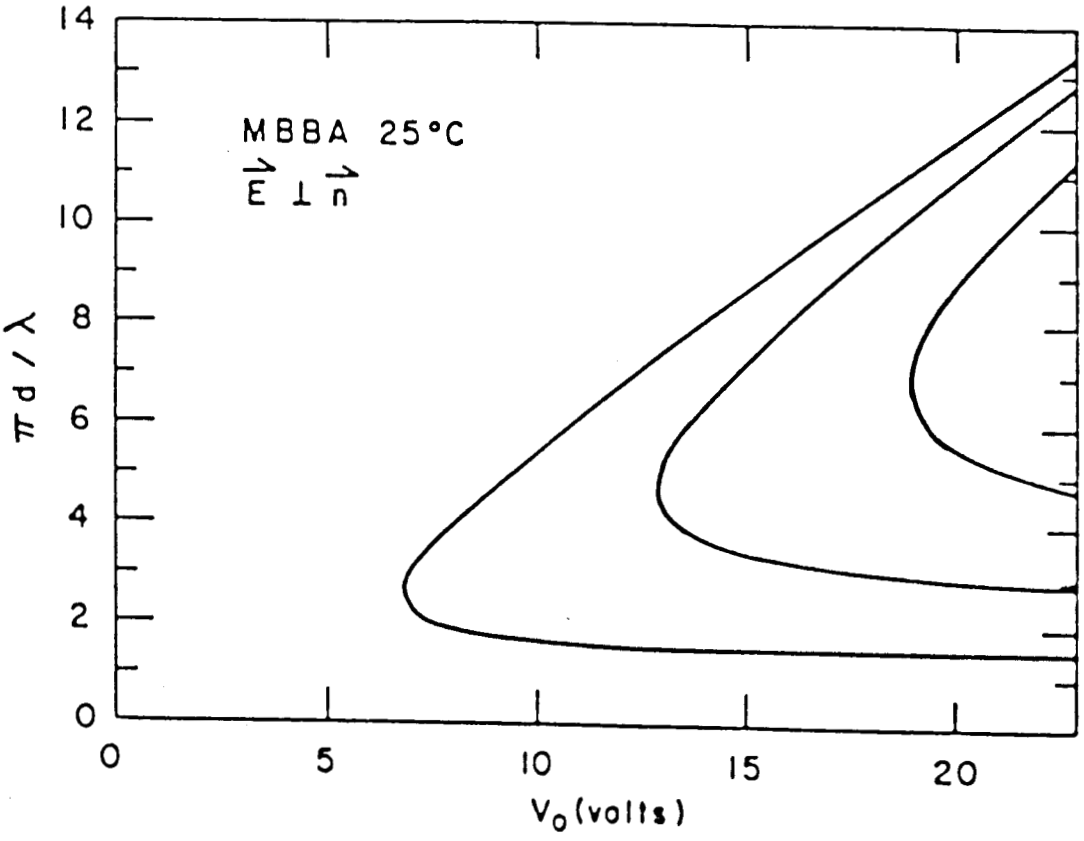

Fig.5. The wavevectors of various normal modes for MBBA as a function of the applied DC voltage, obtained from computer calculations. Note that no solutions exist below about 6.9 Volts. (from Ref.14).

2.4 EXTENSION TO AC EXCITATION

Two different types of EHD instabilities are observed in a nematic with negative ϵ_a under AC electric fields, respectively below and above a certain cut-off frequency f_c . For $f<f_c$ we get the Williams domain instability. It is also known as the conduction regime.

For $f>f_c$, the dielectric regime is observed which is characterized by a field threshold. The optical pattern observed at the threshold consists of a set of parallel striations normal to the initial orientation of the director. The separation between the lines is much smaller than the thickness of the sample. When the field is slightly increased above the threshold value, these striations bend and move to give rise to the 'chevron' pattern (Fig.6). The dielectric regime was first detected by Heilmeir and Helfrich [17], and studied in detail by the Orsay group [9,18].

The variation of the threshold voltage with frequency is shown in Fig.7. The cut-off frequency f_c is typically of the order of 10 - 100 Hz and is found to increase with the conductivity of the sample.

These two regimes of EHD instability in nematics can

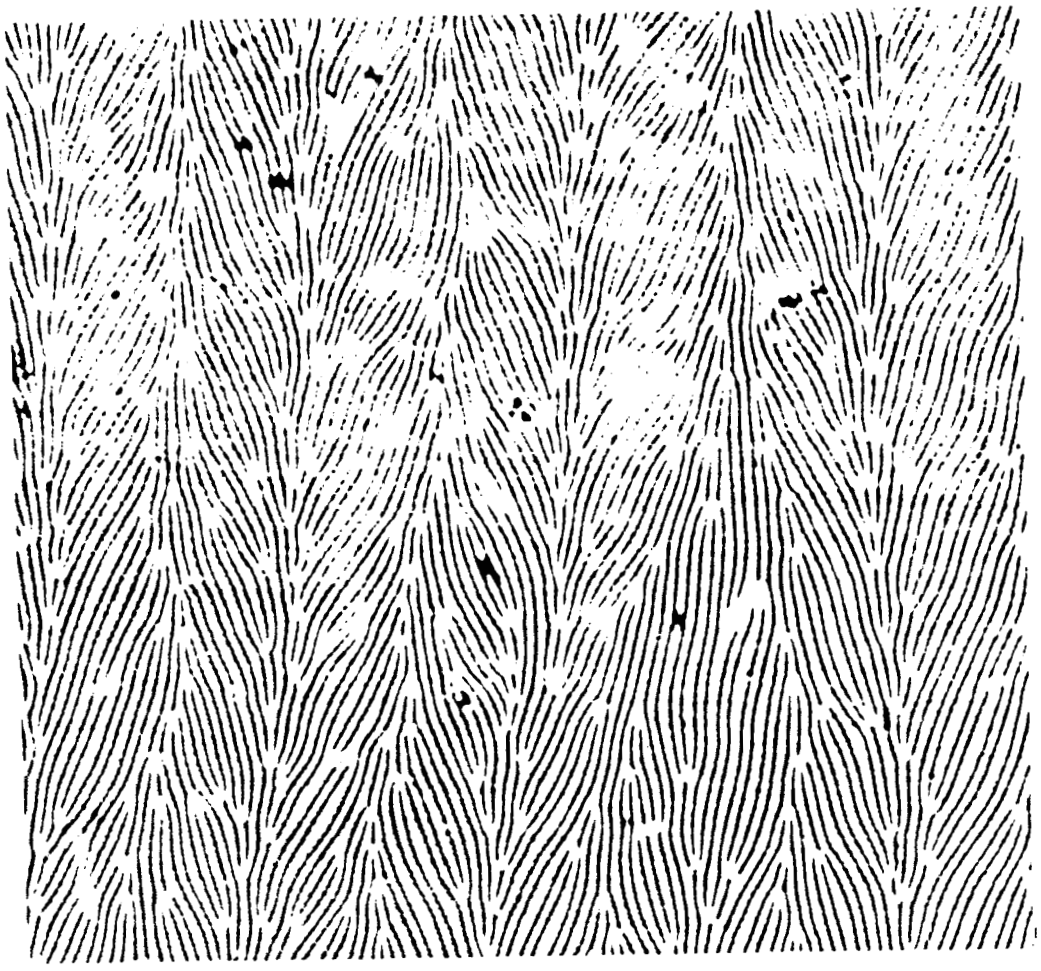

Fig.6. The chevron pattern observed slightly above the threshold in the dielectric regime. (from Ref.16).

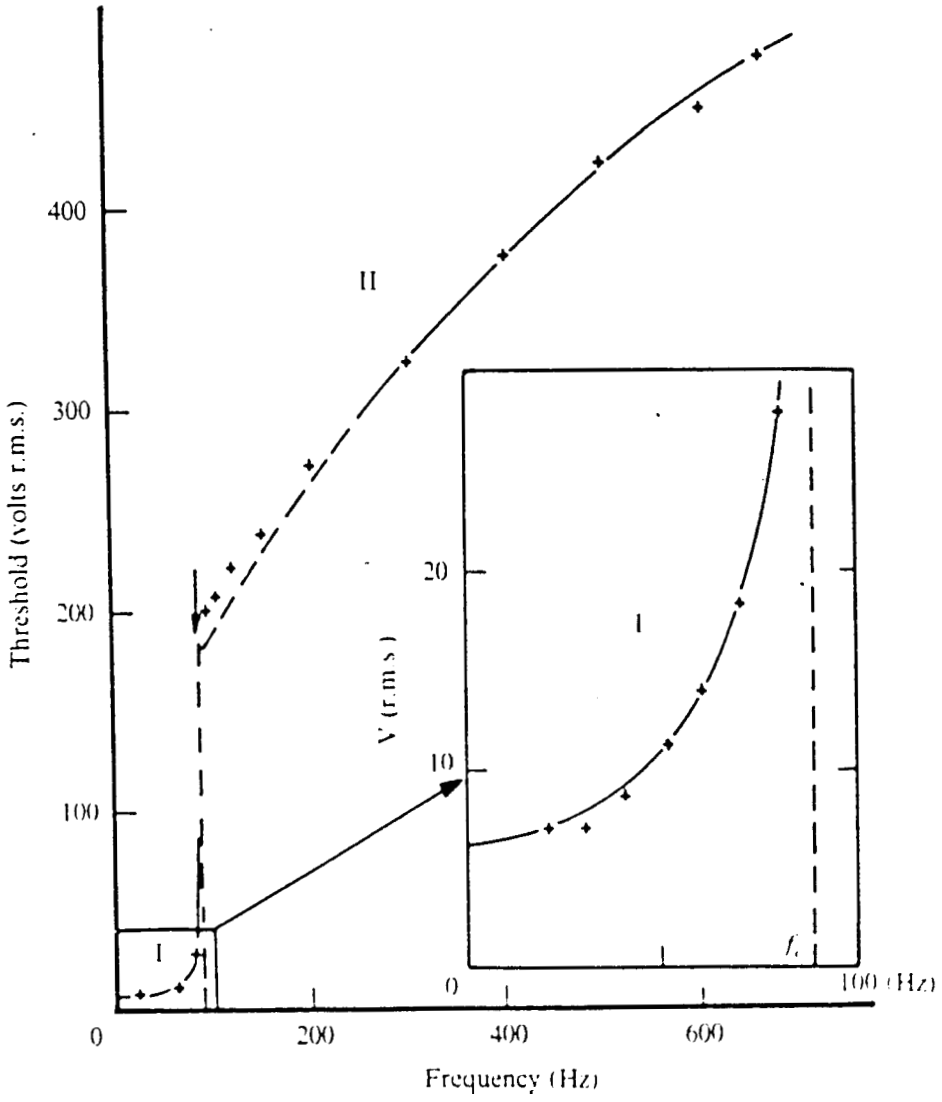

Fig.7. The threshold voltage of the AC instabilities in MBBA as a function of the frequency of the applied field. Regions I and II correspond to the conduction regime and the dielectric regime, respectively. (from Ref.18).

be interpreted in terms of the Carr-Helfrich mechanism, suitably extended to cover time dependent phenomena. A one-dimensional linear analysis for AC excitation was first worked out by Dubois-Violette et al [13] for sinusoidal excitation. A simplified treatment for square-wave excitation was later developed by Smith et al [19]. We shall briefly discuss the latter model, confining our attention to the states of marginal stability of the system.

Including the temporal dependence of all the variables and neglecting the inertial term, a nematic subjected to an AC electric field is described by the following two linearized equations in the curvature $\psi = \partial\theta/\partial x$ and the space charge density Q [13].

$$\dot{Q} + Q/\tau + \sigma_H E_a \psi = 0 \qquad (14)$$

$$\dot{\psi} + \psi/T + (E_a/\eta) Q = 0 \qquad (15)$$

where $1/\tau = 4\pi\sigma_{\parallel}/\epsilon_{\parallel}$ is the relaxation rate of the space charges, $1/T = \eta_1 [K_3 q_x^2 - \epsilon_a \epsilon_{\perp} E_a^2/(4\pi\epsilon_{\parallel})]/(\gamma_1 \eta_2)$ is the relaxation rate of the director field, $1/\eta = -\eta_1 [\epsilon_a/\epsilon_{\parallel} + a_2/\eta_1$ ▮), $\sigma_H = \sigma_{\parallel}(\epsilon_{\perp}/\epsilon_{\parallel} - \sigma_{\perp}/\sigma_{\parallel})$, $\eta_1 = \frac{1}{2}(a_4 + a5 - a2)$ and $\eta_2 = \frac{1}{2}(a_3 + a_4 + a_6) - a_3^2/\gamma_1$.

For a square wave,

$$E_a(t) = \begin{cases} +E & \text{for } 0 < t < 1/(2f) \\ -E & \text{for } 1/(2f) < t < 1/f \end{cases}$$

and the coefficients in the above equations are constants within each half-cycle. Assuming solutions of the form

$$\psi = C_1 \exp(\lambda t/\tau) \quad \text{and} \quad Q = C_2 \exp(\lambda t/\tau),$$

the general solutions are:

$$\psi(t) = a \exp(\lambda_1 t/\tau) + b \exp(\lambda_2 t/\tau) , \tag{16}$$

$$Q(t) = -(\sigma_H E \tau)[\{a/(1+\lambda_1)\} \exp(\lambda_1 t/\tau) + \{b/(1+\lambda_2)\} \exp(\lambda_2 t/\tau)]$$

where,

$$\lambda_{1,2} = -\tfrac{1}{2}(1 + \Gamma\tau) \pm [\tfrac{1}{4}(1 - \Gamma\tau)^2 + \zeta^2(\Gamma\tau - \Gamma_0\tau)]^{1/2}, \tag{17}$$

$= 1$, $\Gamma_0 = \eta_1 K_3 q_x^2 / (\gamma_1 \eta_2)$, $\zeta^2 = \sigma_H \tau / (\eta \Lambda)$ and $\Lambda = -\epsilon_a \epsilon_\perp \eta_1 / (4\pi \epsilon_\parallel \gamma_1 \eta_2)$.

It is clear from Eqs.(14) and (15) that when $\vec{E}_a$ changes sign after every half-cycle, either ψ or Q should reverse its sign. Depending on which one of these two

variables oscillates with the field, we have two distinct physical situations.

1) Q oscillates with the field but ψ does not, ie,

$$Q(t+1/2f) = -Q(t) \text{ and } \psi(t+1/2f) = \psi(t) \qquad (18)$$

This can be realized if we have a static distortion accompanied by the flow of space charges. Hence this regime is called the conduction regime.

2) ψ oscillates with the field but Q does not, ie,

$$\psi(t+1/2f) = -\psi(t) \text{ and } Q(t+1/2f) = Q(t) \qquad (19)$$

In other words, the curvature in the director field oscillates with the field and the space charges maintain their sign. This is called the dielectric regime. Substituting the general solution in Eq.(18) we get the following threshold condition for the conduction regime.

$$(1+\lambda_1) \tanh(\lambda_1/4f\tau) = (1+\lambda_2) \tanh(\lambda_2/4f\tau) \qquad (20)$$

Similarly for the dielectric regime, we get

$$(1+\lambda_1) \tanh(\lambda_2/4f\tau) = (1+\lambda_2) \tanh(\lambda_1/4f\tau) \qquad (21)$$

Substituting for λ_1 and λ_2 in Eqs.(20) and (21), we find that in the conduction regime

$$\Delta \sinh[1/(4fT) + 1/(4f\tau)] = (1 - \tau/T) \sinh(\Delta/4f\tau) \qquad (22)$$

and in the dielectric regime

$$\Delta \sinh[1/(4fT) + 1/(4f\tau)] = (\tau/T - 1) \sinh(\Delta/4f\tau) \qquad (23)$$

where $\Delta = [(1-\Gamma\tau)^2 + 4E^2\zeta^2\tau\Lambda]^{1/2}$. It is clear from Eqs.(22) and (23) that the condition $T = \tau$ splits the problem naturally into two parts. For $T > \tau$ there is no solution to Eq. (23) and consequently no dielectric regime. For $T < \tau$ there is no solution to Eq.(21) and hence no conduction regime.

In order to solve the problem it is necessary to find a pair of eigenvalues λ_1 and λ_2 which satisfy Eq.(17) and either Eq.(20) or Eq.(21). For each frequency those values of E are to be found which give such pairs of eigenvalues. These E values define the states of marginal stability of the system. The stability diagram giving the threshold voltage as a function of frequency is shown in Fig.8 . Along branch (a) the system becomes unstable with respect to the conduction regime and along the branch (c)

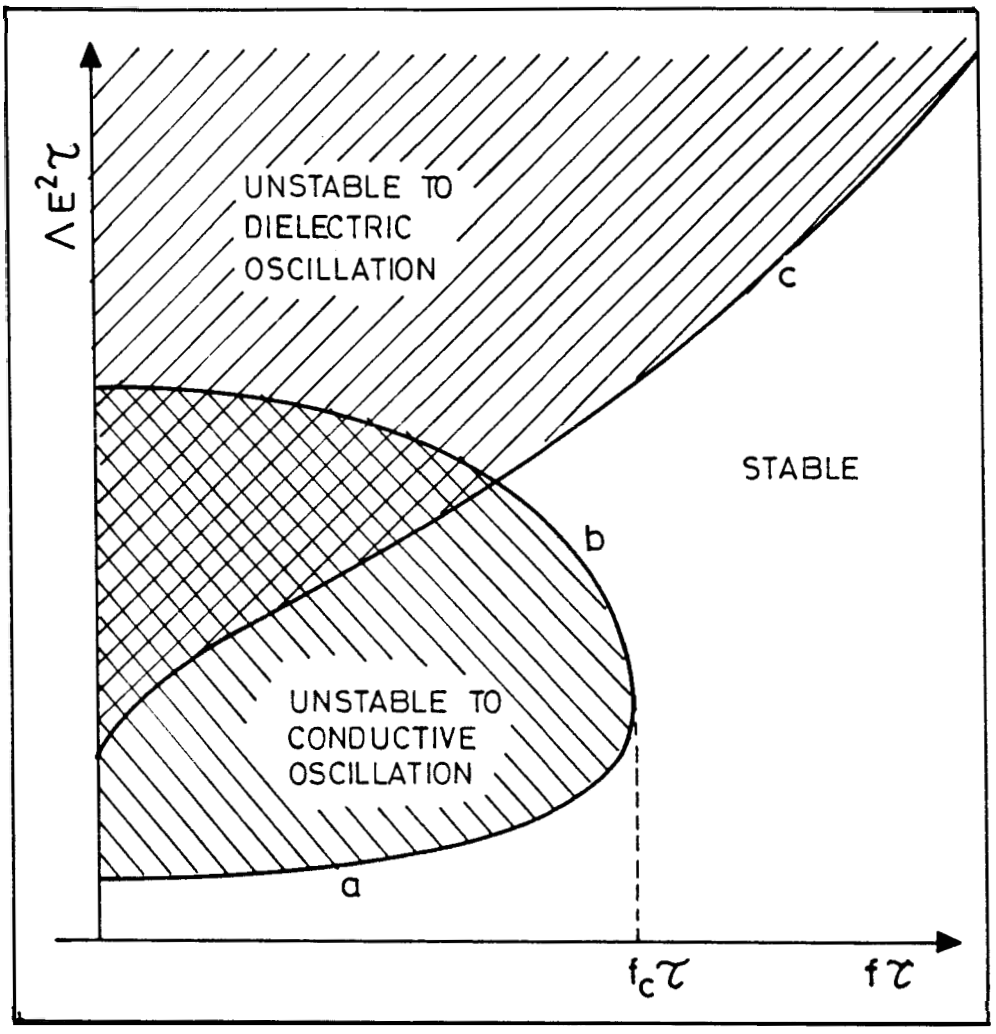

Fig.8. The variation of the threshold field with the frequency of the applied electric field, obtained from numerical calculations. The curves labelled a, b and c correspond to the onset of the conduction regime, the restabilization branch and the onset of the dielectric regime, respectively. (from Ref.19).

with respect to the dielectric regime. Along branch (b) the system again becomes stable with respect to the conduction regime. Thus the conduction regime is confined to a closed region in the (E, f) plane. The cut-off frequency of the conduction regime is given by $f_c \approx 1/2\pi\tau$. As mentioned earlier, the conduction regime can exist only if the director relaxation time T is larger than the charge relaxation time τ, so that space charges can develop in the medium. T decreases with increase in E (see Eq.15) and along the restabilization branch (b) T becomes comparable to τ. Above this branch $T < \tau$ and the conduction regime does not exist. On the other hand, the condition for the existence of the dielectric regime is that $T < \tau$. This can always be achieved by increasing $\vec{E}$ as ϵ_a is negative. Hence solutions corresponding to the dielectric regime exist for all frequencies.

The dielectric and restabilization branches are characterized by field thresholds whereas the conduction regime sets in at a threshold voltage. Consequently, as the thickness d of the nematic layer is decreased, the restabilization branch approaches the conduction branch and at some value of d they become equal. The conduction regime cannot be observed if d is below this minimum value given by

$$d_{min} = \pi \left[\epsilon_{\parallel} K_3 \zeta^2 \eta_1 / \{4 \pi \sigma_{\parallel} \tau_1 \eta_2 (\zeta^2 - 1)\} \right]^{1/2}$$

The above analysis being one-dimensional, cannot predict a nonzero value of the wavevector of the rolls in the conduction regime. As in the Helfrich model we have to assume that $q = \pi/d$ at the threshold. On the other hand, the theory predicts the wavevector of the rolls in the dielectric regime. For low-frequencies it is given by

$$q^2 \propto (1/\zeta^2) [\zeta^2 - 1 + 4 f\tau \{ \zeta^2 - 1 + \ln 2 f\tau \}]$$

All the above mentioned predictions of the theory have been found to be in good qualitative agreement with the experiments [3].

A simple numerical procedure which allows a convenient and exact calculation of the threshold curves and instability regions in the context of a one-dimensional model was developed by Sengupta and Saupe [20]. Taking $\vec{E}_a = \vec{E}_o \cos(\omega t)$, Eqs.(14) and (15) form a system of linear differential equations with periodic coefficients. It follows from the Floquet theory [21] that their solutions can be expressed in the form

$$\theta(t) = \exp(\mu t) \sum_n a_n \exp(in\omega t)$$
$$Q(t) = \exp(\mu t) \sum_n b_n \exp(in\omega t) \qquad (24)$$

with $n = \pm 1, \pm 2$, etc. Here μ is a characteristic exponent and is assumed to be real. The condition Re $\mu = 0$ defines the states of marginal stability of the system. It can be directly verified that if $\theta(t)$ and $Q(t)$ are solutions, then $\theta(t+1/2f)$ and $-Q(t+1/2f)$ or $-\theta(t+1/2f)$ and $Q(t+1/2f)$ are also solutions, f being the frequency of the applied field. This ensures that the coefficients a_n and b_n in Eq.(24) satisfy the following relations:

$$a_{2n+1} = b_{2n} = 0 \; ; \; a_{2n} = b_{2n+1} = 0 \qquad (25)$$

In the first case, therefore, $\theta(t)$ does not change sign with the field but $Q(t)$ does. These even modes correspond to the conduction regime. In the second case, $\theta(t)$ changes sign with $\vec{E}$ but $Q(t)$ does not. These odd modes correspond to the dielectric regime.

Using the solutions (24) in Eqs. (14) and (15), the following recurrency relations can be obtained.

$$M_{n,n-1} a_{n-2} + M_{n,n} a_n + M_{n,n+1} a_{n+2} = 0 \qquad (26)$$

with $M_{n,n} = \tau/T + (\mu + in\omega)\tau + M_{n,n-1} - M_{n,n+1}$,

$M_{n,n\pm1} = (e^2/2)[1 - 1 \quad (\omega_c\tau)^2\}/\{1 + \mu\tau + i\,(n \pm 1)\omega\tau\}]$,

$e^2 = -\tau\,\epsilon_a\,\epsilon_\perp\,E_o^2 \,/(\,8\,\pi\,\epsilon_{||}\,\eta_b\,)$ and

$(\omega_c\tau)^2 = (\epsilon_{||}/\epsilon_a)[1-\epsilon_{||}\,\sigma_\perp/(\epsilon_\perp\,\sigma_{||})](\epsilon_a/\epsilon_{||} + \alpha_2/\eta_1) - 1$

and $\eta_b = \gamma_1 - \alpha_2^2/\eta_1$

Eq.(26) can be solved using the method of continued fractions. Convergent solutions exist only for suitable sets of parameter values. Taking = 0, the threshold field is obtained in terms of ω, ω_c and τ/T.

2.5 OBLIQUE-ROLL INSTABILITY

All the theoretical investigations described above assume that the convection rolls are normal to the undistorted director $\hat{n}_o$. Recently, however, there have been a few experimental observations of oblique rolls whose wave vector makes an angle a with $\hat{n}_o$, both under DC and very low frequency AC excitation [22-24] (Fig.9). Detailed experiments on the oblique-roll instability were carried out by Ribotta et al. [24]. They obtained similar results both with MBBA and a commercially available nematic mixture, viz, Merck phase V. Their quantitative measurements which have been reported only on Merck phase V are summarized below.

- At low frequencies of excitation oblique rolls are formed

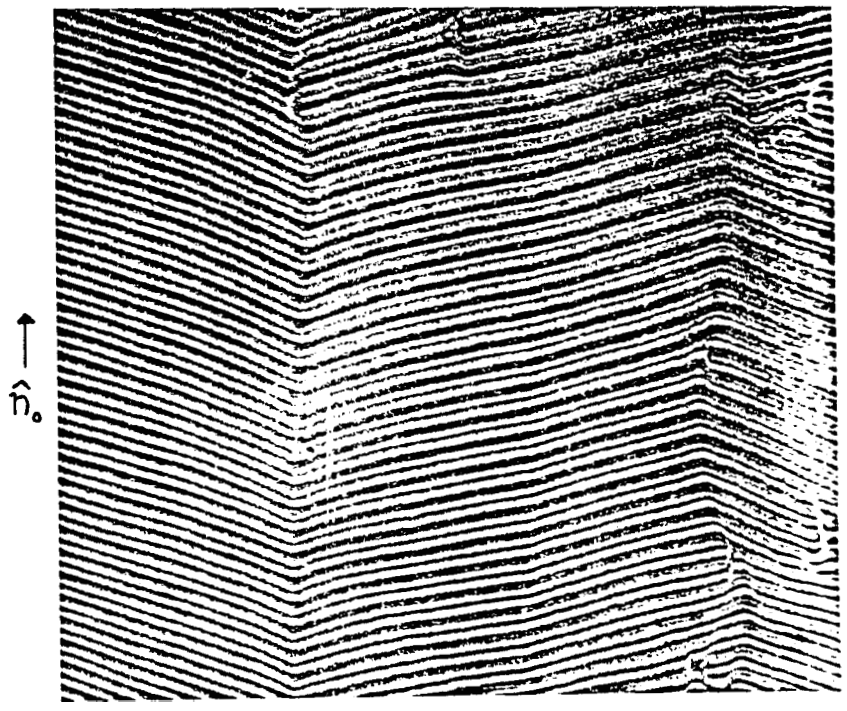

Fig.9. Oblique-rolls observed in a 6 μm thick sample of Merck phase 5A. 5.39 V, 50 Hz. (from Ref.22).

right at the threshold of the instability. For example, at f=10 Hz they find a ≈ 30'.

-The oblique rolls are obtained at the threshold only upto a critical frequency f_o (Fig.10). For the sample they studied the cut-off frequency f_c was 120 Hz and $f_o \approx 40$ Hz.

-f_o increases with the conductivity of the sample.

-f_o decreases when a stabilizing magnetic field is applied along $\hat{n}_o$.

-Tracer particles flow along open helical trajectories within the rolls. The axial component of the particle velocity in adjacent rolls has opposite directions.

-Beyond f_o normal rolls are obtained at the threshold in the conduction regime. But as the field is further increased they first become undulatory and then oblique (Fig.10)

The Helfrich-Orsay one-dimensional analysis of the problem cannot account for these oblique rolls. This can be clearly seen by extending the Helfrich model for DC excitation to the case of oblique rolls. Let $\hat{n}_o$ be along the X-axis. On applying an electric field along Z, let the rolls be formed along ξ, making an angle a with the X-axis. In the distorted state the director orientation is defined by the polar angles θ and Φ (see Fig.11). The equations describing the system are

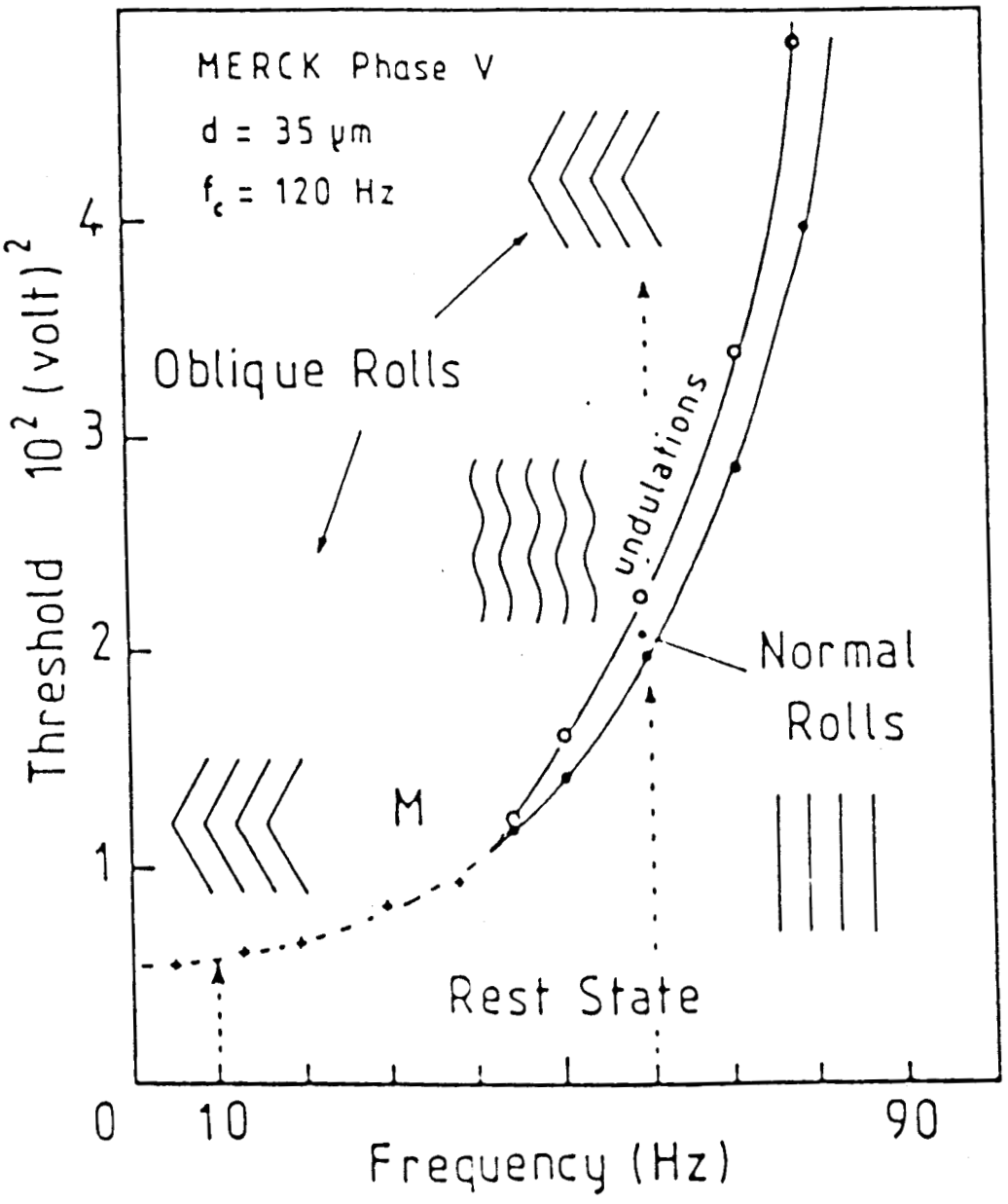

Fig.10. The stability diagram giving the variation of the threshold field with the frequency of the applied electric field. Below the triple point M oblique-rolls are obtained at the threshold. Beyond M, normal-rolls are obtained first and as the field strength is raised, they become undulatory and then change continuously into oblique-rolls. (from Ref.24).

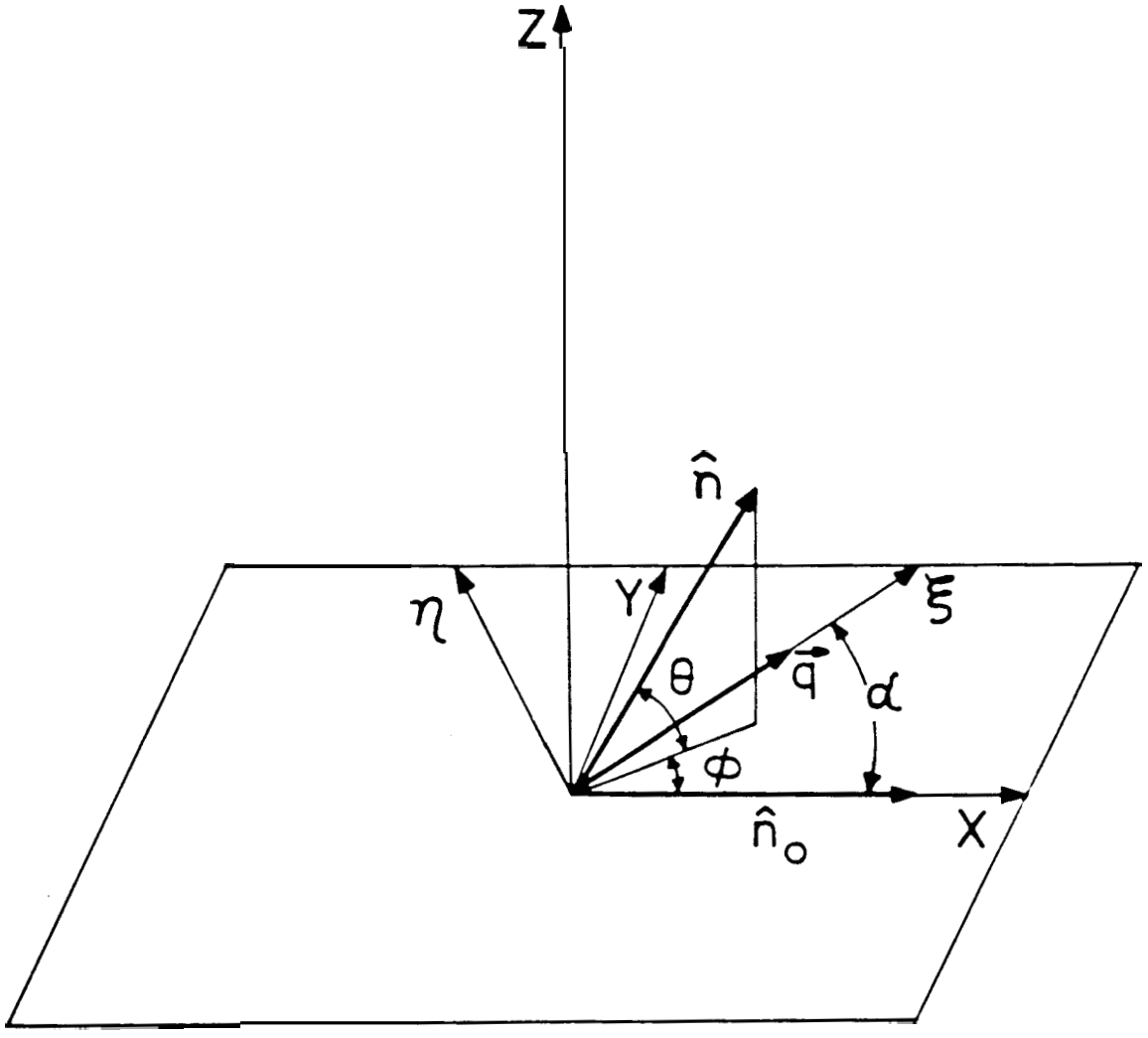

Fig.11. Illustration of the coordinate system and definitions of the angles used in the text.

$$M\,(d^2\theta/d\xi^2)+[\epsilon_a\sigma_\perp/(4\pi\sigma_c)+a_2\epsilon_c(\epsilon_r-\sigma_r)c^2/(4\pi\eta_1)]\,E_a^2\theta = 0 \qquad (27)$$

$$L\,(d^2\Phi/d\xi^2) = 0 \qquad (28)$$

where, $M = K_2 s^2 + K_3 c^2$, $L = K_1 s^2 + K_3 c^2$, $\sigma_c = \sigma_\perp + \sigma_a c^2$, $\epsilon_c = \epsilon_\perp + \epsilon_a c^2$, $\sigma_r = \sigma_a/\sigma_c$, $\epsilon_r = \epsilon_a/\epsilon_c$, $\eta_1 = \frac{1}{2}[a_4 + (a_5 - a_2)c^2]$, s = sin a and c = cos a.

Assuming solutions of the form

$$\theta = \theta_0 \cos(\vec{q}.\vec{r}) \text{ and } \Phi = \Phi_0 \sin(\vec{q}.\vec{r}),$$

consistent with the symmetry of the problem, we find from Eq.(28) that $\Phi = 0$ and hence a = 0.

A possible explanation for the existence of oblique rolls at very low frequencies in the conduction regime was first proposed by Zimmermann and Kramer [25], who showed that the oblique rolls can be obtained if the boundary conditions are taken into account. In order to simplify the problem and to get an analytical expression for the threshold voltage the boundary conditions were assumed to be stress-free in their analysis. The geometry considered is shown in Fig.12a. $\hat{n}_o$ is along the X-axis, the external electric field $\vec{E} = \vec{E}_o \cos(\omega t)$ along Z and a

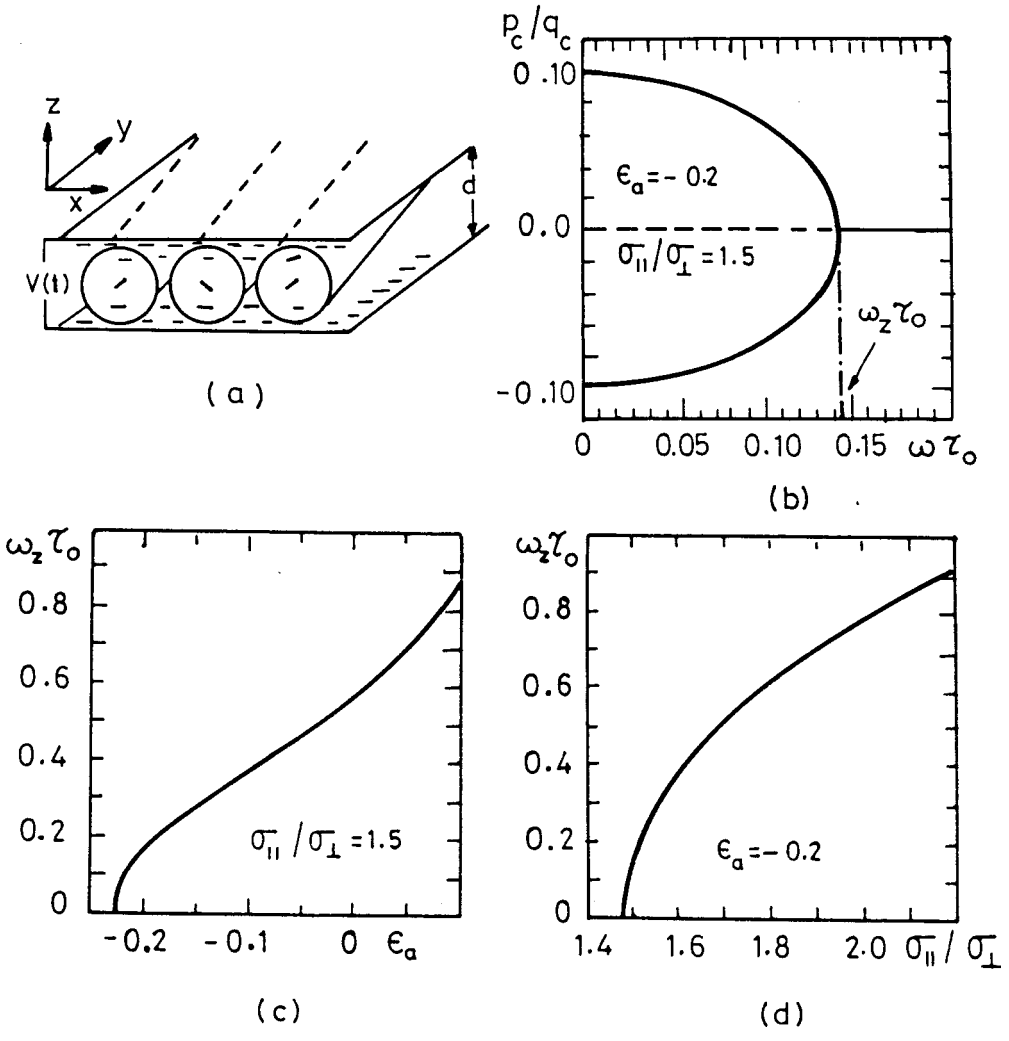

Fig.12. (a) The geometry considered. (b) The pitchfork bifurcation in the $p_c/q_c - \omega\tau_o$ plane for MBBA. (c), (d) The dependence of the critical frequency ω_z on ϵ_a and $a,,/\sigma_\perp$. (from Ref.25).

magnetic field $\vec{H} = (H_x, H_y, H_z)$ is applied in an arbitrary direction. The EHD equations describing the system allow the following solutions [25] :

$$
\begin{aligned}
v_{x,y} &= A_{1,2} \sin z \cos(qX + pY) \\
v_z &= A_3 \cos z \sin(qX + pY) \\
\psi_{1,2} &= A_{4,5} \cos z \sin(qX + pY) \\
\theta &= A_6 \cos z \cos(qX + pY) \\
\Phi &= A_7 \sin z \sin(qX + pY)
\end{aligned}
\qquad (29)
$$

where $\vec{v}$ is the velocity, θ and Φ are the polar angles describing the director orientation and $\psi = \psi_1 \cos(\omega t) + \psi_2 \sin(\omega t)$ is the electric potential. Further all lengths are measured in units of π/d. It is clear that v_x, v_y and Φ are not zero at the boundaries and as mentioned earlier, the boundary conditions correspond to an unrealistic stress-free surface. Using the above solutions an analytical expression for the threshold voltage can be obtained.

$$
V_o^2 = \pi^2 (1+\omega^2 \tau^2)[L_2 - p^2 (K_1 - K_2)^2 / L_1] / [\epsilon_a \epsilon_o \{q^2 F M_1 + (q^2+P)G\}]
$$

where, $L_1 = K_1 p^2 + K_2 + K_3 q^2 + d^2 \chi_a \mu_o (H_x^2 - H_y^2) / \pi^2$,

$L_2 = K_1 + K_2 p^2 + K_3 a' + d^2 \chi_a \mu_o (H_x^2 - H_z^2) / \pi^2$,

$S = q^2 \sigma_{11} / \sigma_\perp + P$, $D = q^2 \epsilon_{11} / \epsilon_\perp + P$, $P = 1 + p^2$, $\tau = \tau_o D / S$,

$\tau_o = \epsilon_o \epsilon_\perp / \sigma_\perp$, $M_2 = p^2[(a_3 p^2 - a_2 q^2)\beta_1 - a_3 \beta_2](K_1 - K_2) / L_1$,

$M_3 = -a_3 \beta_1 p^2 + (a_3 - a_2 q^2)\beta_2$, $M_1 = (M_2 + M_3)/(\beta_2 \beta_3 - \beta_1^2 p^2)$,

$\beta_1 = \beta - \frac{1}{2} a_4 q^2$, $\beta = \eta_2 P + (\eta_1 + \eta_2 + a_1) q^2$,

$\beta_2 = \frac{1}{2} a_4 q^2 + \beta p^2 + \eta_1 q^4$, $\beta_3 = \beta + \frac{1}{2} a_4 q^2 p^2 + \eta_1 q^4$,

$\eta_1 = \frac{1}{2}(a_4 + a_5 - a_2)$, $\eta_2 = \frac{1}{2}(a_3 + a_4 + a_6)$,

$F = [\sigma_a \epsilon_\perp D / (\epsilon_a \sigma_\perp S)] - 1$ and $G = (D/S + \omega^2 \tau^2)/D$.

This model leads to the following results : Though oblique rolls are not obtained for the standard values of the material parameters of MBBA, they can be obtained by varying suitably any one of the parameters, keeping the others fixed. For example, a non-zero value of a can be obtained at $\omega = 0$ and $\vec{H} = 0$ by taking $\epsilon_a \geq -0.226$ instead of the standard MBBA value of -0.5.

As the frequency f of the applied field is increased, a decreases and goes to zero at a critical frequency f_o. Fig.12b shows the variation of p_c / q_c (= tan a) with the frequency. Here, a non-zero value of a is obtained by taking $\epsilon_a = -0.2$. Figs.12c and 12d show $\omega_z \tau$ (where $\omega_z = 2\pi f_o$ and $\tau_o \equiv \epsilon_\perp/(4\pi\sigma_\perp)$) as functions of $a_{,,}/\sigma_\perp$ and $\epsilon_{,}$, respectively. As mentioned earlier, quantitative measurements on the oblique roll instability in MBBA are not available. Also, not all material parameters of Merck phase V are known. Hence in order to compare their theory

with experiments Zimmermann and Kramer calculate f_o by first estimating a from fitting the theoretical cut-off frequency f_c to the experimental value of Ribotta et al. [24], taking ϵ_a = - 0.2 and standard MBBA values for the other parameters. They get f_o = 5.25 Hz whereas Ribotta et al. find $f_o \approx$ 40 Hz. Though the above analysis gives a plausible explaination for many experimental observations on the oblique-roll instability in nematics, it is not entirely satisfactory, as reflected hy the relatively small value of f_o predicted by it. The results of the above analysis are in agreement with those of a full three-dimensional model for DC excitation developed by us which takes into account the rigid boundary conditions [26]. This model is discussed in chapter 4. Very recently Bodenschatz et al.[27] have also made detailed calculations taking into account the rigid boundary conditions, for both DC and AC excitation.

Oblique rolls are also found in the dielectric regime, though they are not expected on the basis of the Orsay model. The chevron pattern [3,9] obtained just above the threshold consists of oblique rolls whose wavevector makes a large angle ($\sim 30^\circ$) with the direction of initial orientation of the director (Fig.6).

2.6 EHD INSTABILITIES IN NEMATICS WITH NEGATIVE CONDUCTIVITY ANISOTROPY

Another experimental observation that cannot be accounted for by the theoretical models described above is the occurrence of EHD instabilities in nematics with negative conductivity anisotropy. In some nematics, at temperatures close to the nematic - smectic transition point the conductivity anisotropy changes sign due to the smectic - like short range order in the medium [28] (Fig.13). It was shown by Dubois-Violette et al.[13] that the Carr-Helfrich mechanism can operate only if the parameter

$$\zeta^2 = [1 - \sigma_\perp \epsilon_\parallel / (\sigma_\parallel \epsilon_\perp)]\ [1 + a_2 \epsilon_\parallel / (\eta_1 \epsilon_a)]$$

where $\eta_1 = \frac{1}{2}(a_4 + a_5 - a_2$, is greater than 1. In materials with $\sigma_\perp > \sigma_\parallel$ and small enough negative ϵ_a , $\zeta^2 < 1$ and this mechanism can not operate. Nevertheless, homogeneously aligned samples of materials with $\zeta < 1$ exhibit two types of EHD instabilities [29-31], below and above a critical frequency f_c . The materials used by Gosciansky [29] are n-(p-butoxybenzylidene)-p-n-octylaniline (40.8) and 4-4' octyloxyazoxybenzene (C8) . The former compound exhibits a S_A -N transition while the latter shows a S_C -N transition. Blinov et al. [31] used three homologues of 40.8 in their studies. In all these five materials a_1 is

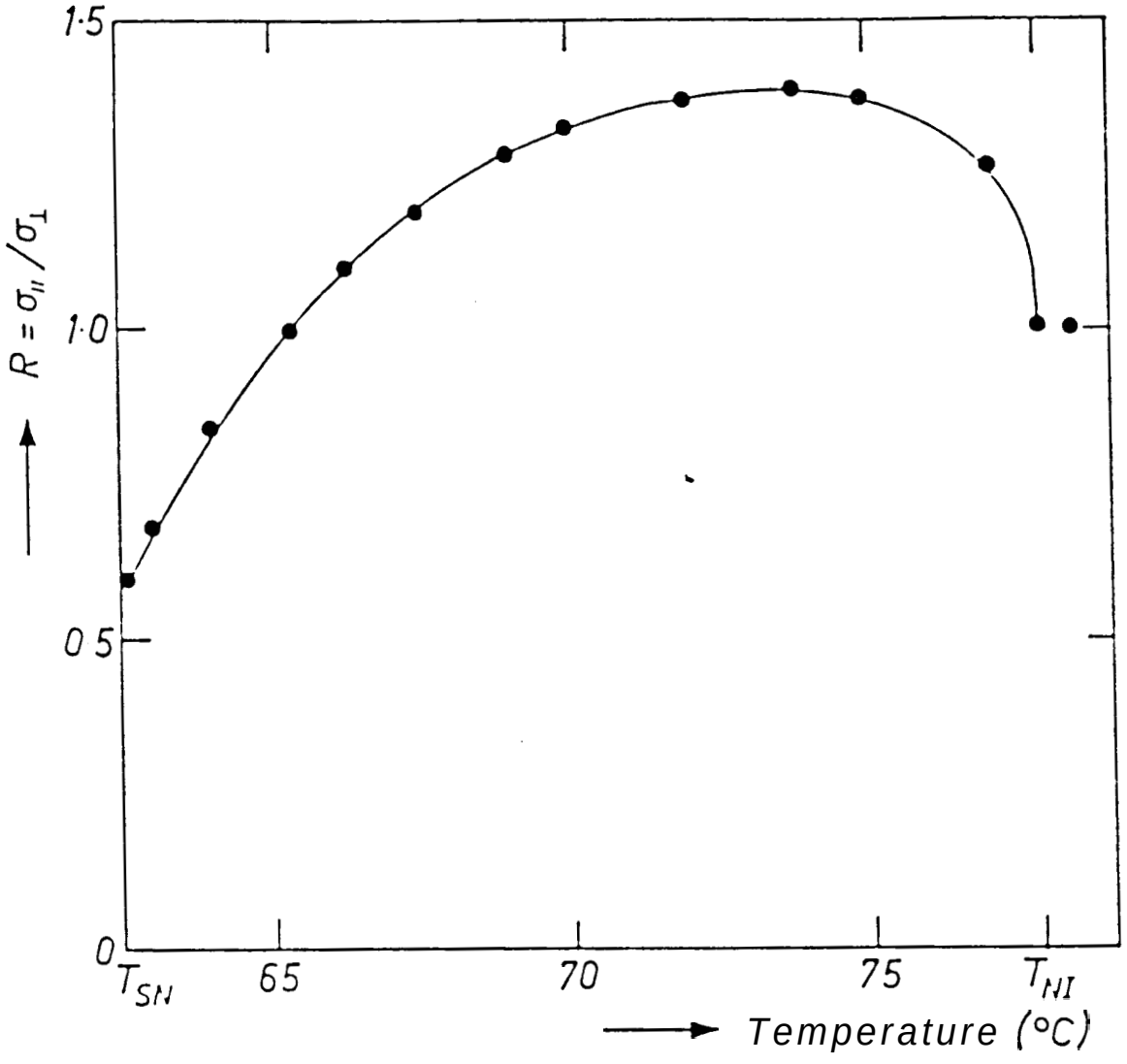

Fig.13. Variation of the ratio R= $\sigma_{\parallel}$ /$\sigma_{\perp}$ in the nematic phase of 40.8. (from Ref.30).

negative in a temperature range $T_{NS} < T < T^*$ in the nematic phase and similar observations are reported in all of them, which are summarized below.

A. The low frequency regime:

- The instability is characterized by a field threshold (Fig. 14).
- At the threshold convection rolls appear with their axes making a small angle with $\hat{n}_o$ (Fig.15). Hence they are generally referred to as longitudinal domains.
- The width of the rolls is comparable to the sample thickness.
- Tracer particles move along helical trajectories within the rolls.
- Analysis of the time dependence of the light diffracted by the domains indicate oscillations of the curvature of the director field.
- The threshold field is not very sensitive to the frequency at low frequencies, but increases sharply as the frequency approaches f_L .
- If the sample thickness is sufficiently small this instability has a lower threshold than the Williams domains even in the temperature range where $\sigma_a > 0$, at low frequencies.
- At very low frequencies (—10 Hz) the threshold field is proportional to $\sigma^{1/2}$, a being the mean conductivity of

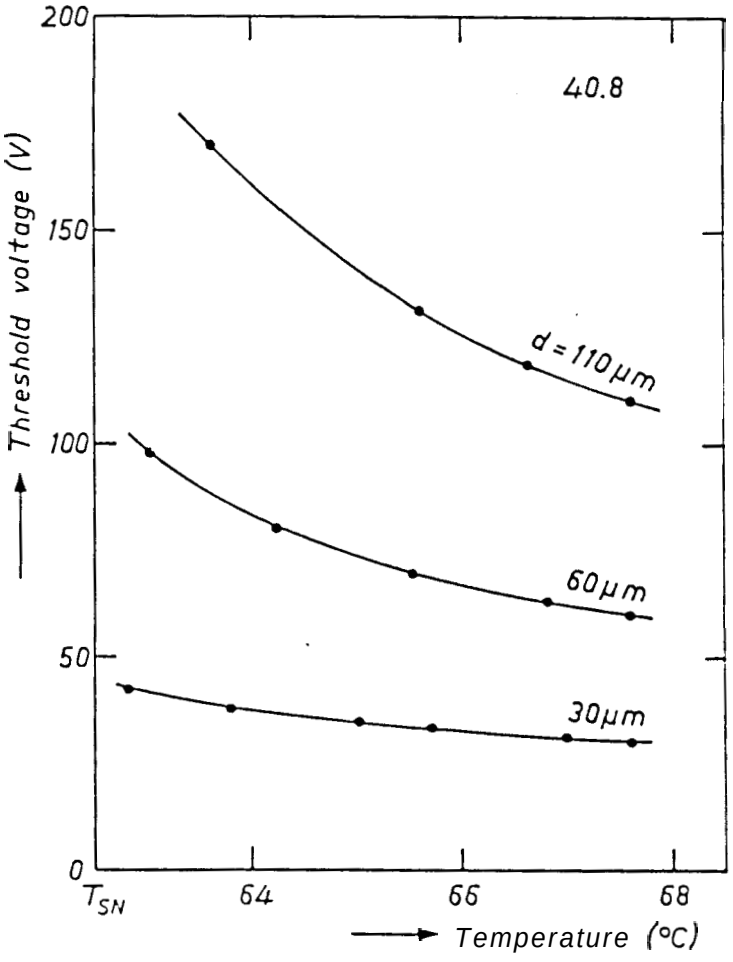

Fig.14. Variation of the threshold voltage for the longitudinal domains with temperature. Note that the threshold voltage increases almost linearly with the sample thickness. (from Ref.30).

the sample.

-The threshold field is insensitive to small variations in σ_a and ϵ_a .

B. The high frequency regime:

-As in the low frequency regime the instability is characterized by a field threshold.

-Unlike in the low frequency regime the periodicity of the convective structure is much less than the sample thickness.

-While Blinov et al. [31] find linear domains directed arbitrarily in the medium, Goscianski [29,30] reports a square grid pattern at the onset of the instability (Fig.16).

-The threshold field varies linearly with $f^{1/2}$ (Fig.17).

-Analysis of the diffracted light indicates that the curvature of the director oscillates with the field.

-As the temperature is raised the threshold field gradually decreases and does not show any discontinuity at T*, where σ_a changes sign (Fig.18). However, at T>T*, the pattern corresponding to the dielectric regime in materials with $\sigma_a > 0$ is obtained.

-The threshold field is independent of the average conductivity o. It is also not sensitive to small variations in σ_a and ϵ_a .

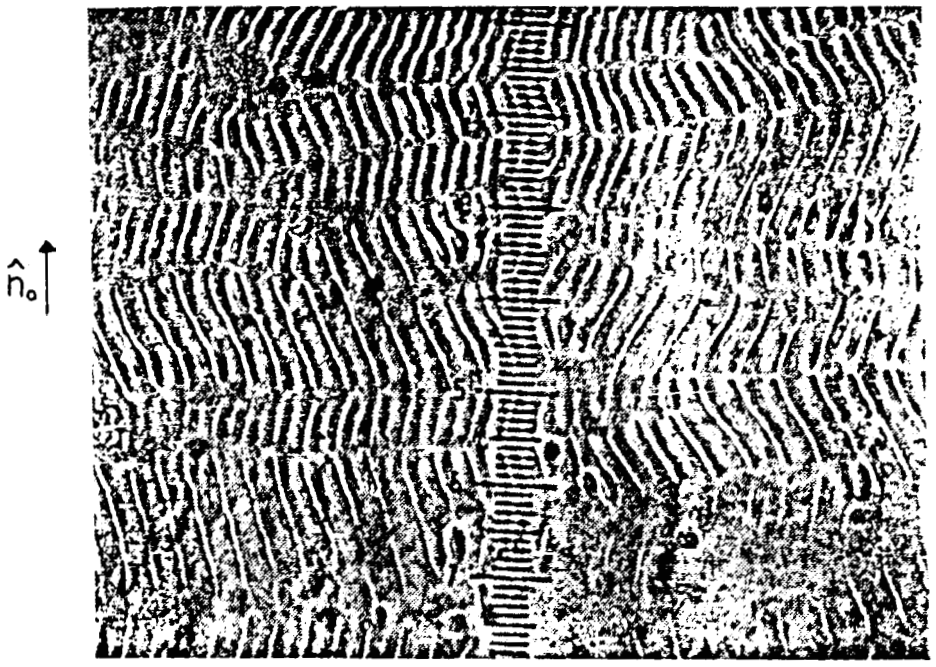

Fig.15. The low frequency 'longitudinal' domains observed in a 30 μm thick sample of C8 at T =115° C (T* =118° C). (from Ref.29).

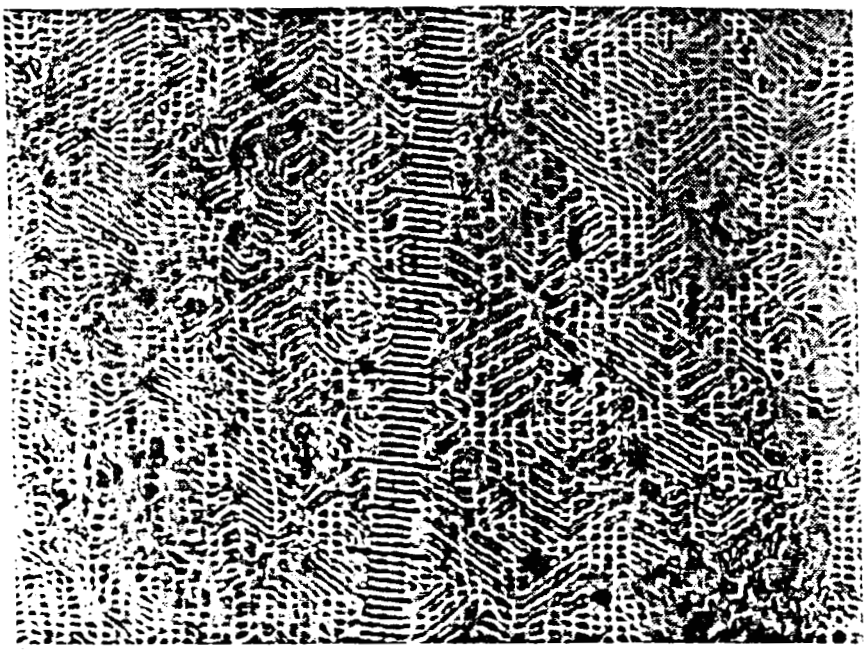

Fig.16. The bidimensional pattern observed at high frequencies in a 30 μm thick sample of C8 at T = 115° C. (from Ref.29).

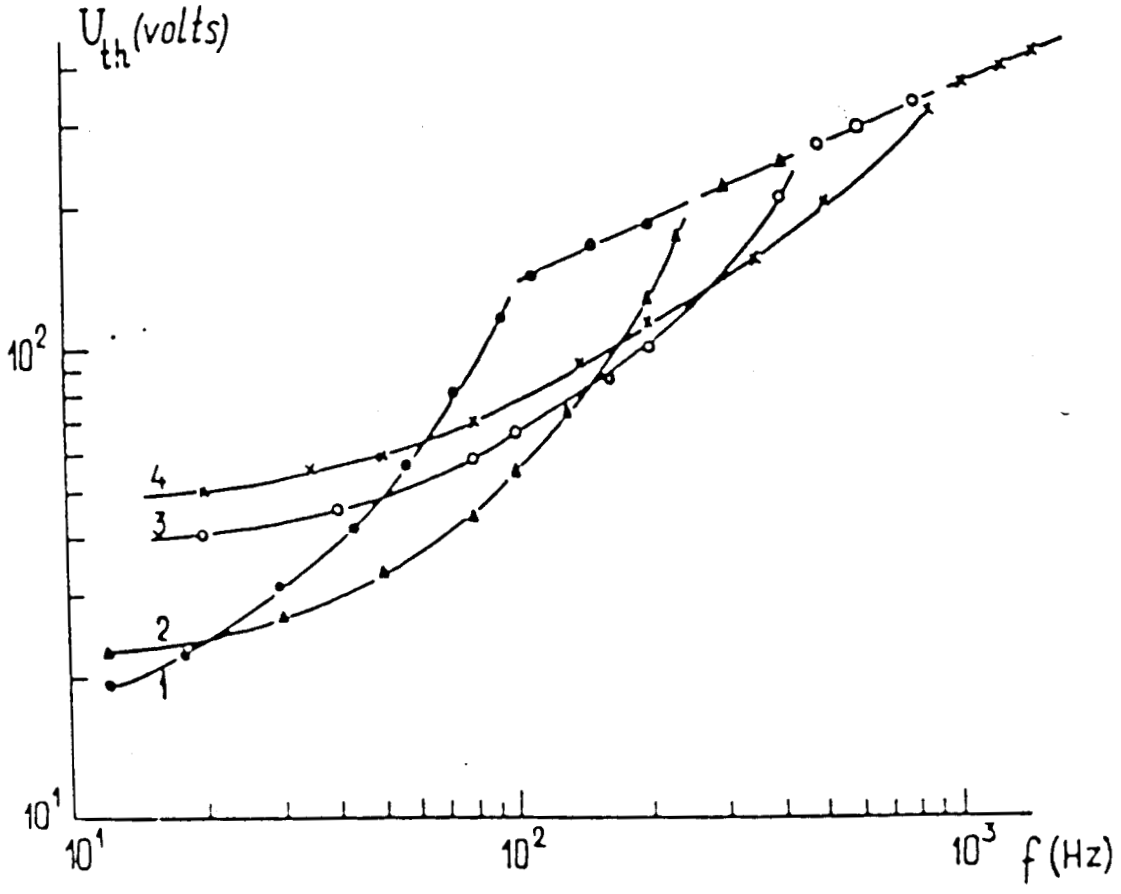

Fig.17. Frequency dependence of the threshold voltages for a homogeneously aligned layer of 40.4 at T = 47°C (T* = 51°C) . d=30 μm. Electrical conductivity: 8 x10^{-11} (1), 1.5 x10^{-10} (2), 3 x10^{-10} (3) and 5 x10^{-10} ohm-1 cm^{-1} (4). (from Ref.31).

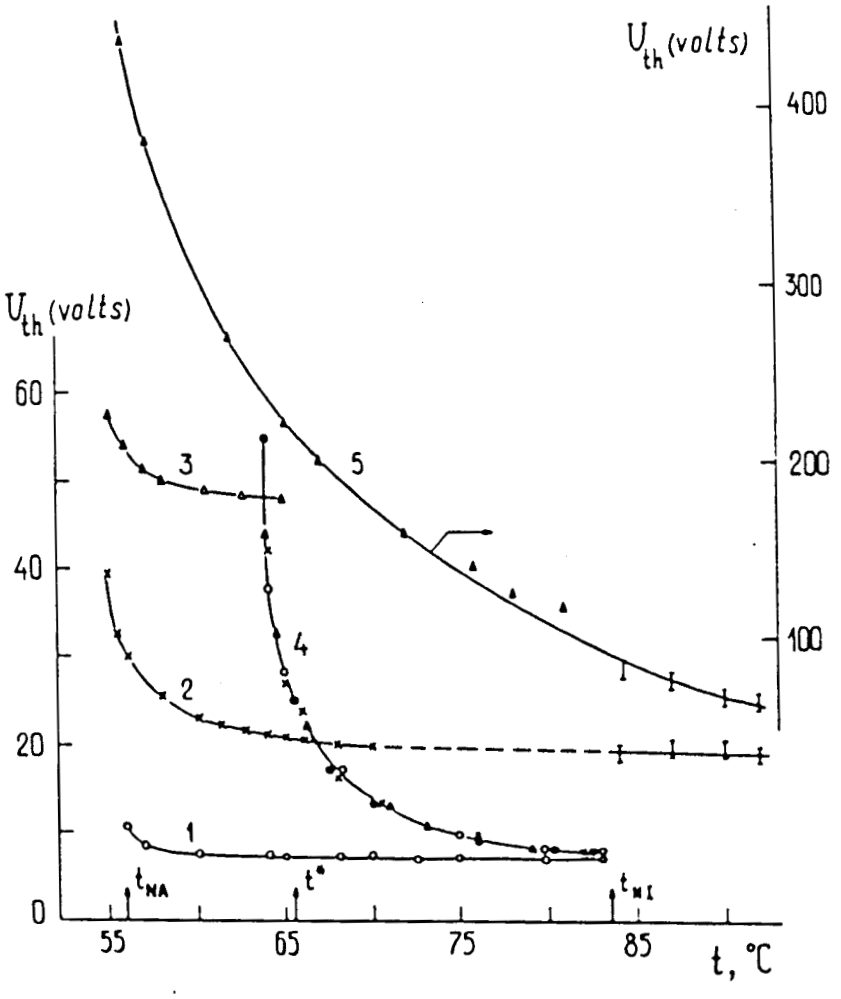

Fig.18. Temperature dependences of the threshold voltages of EHD instabilities in a homogeneously aligned layer of 40.7. 1,2,3: the low frequency longitudinal domains at d = 10, 30, 65 μm, respectively and f< 20 Hz. 4: Williams domains at f< 20 Hz. 5: High frequency instability at f = 1 KHz and d = 30 μm. (from Ref.31).

Blinov et al. [31] invoke the isotropic mechanism to account for these instabilities. This mechanism is discussed in the following section.

2.7 ALTERNATIVE MECHANISMS FOR EHD INSTABILITIES IN NEMATICS

EHD instabilities are also observed in weakly conducting isotropic liquids both under DC and AC excitation [3]. A mechanism for the DC instability was proposed by Felici [32], based on unipolar charge injection from one of the electrodes. Such charge injection leads to a non-uniform distribution of space charges along the field direction (Fig.19). The force due to the external field on this space charge distribution is destabilizing and gives rise to a cellular flow in the medium when the field is sufficiently large. The Felici instability is analogous to the Benard instability [1], where convection sets in due to the action of the gravitational field on a vertical density gradient. The Felici mechanism gives a threshold voltage [3]

$$V_{th} = T\, 4\pi\eta\mu/\epsilon$$

where η is the viscosity, ϵ the dielectric cdnstant and μ the mobility of the charge carriers. The coefficient T was computed by Atten and Moreau [33] to be 161.

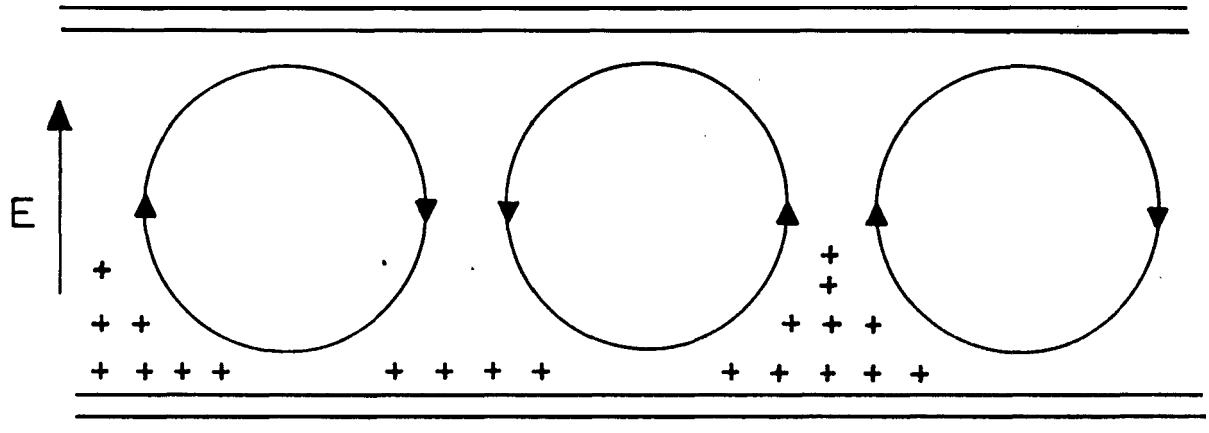

Fig.19. Schematic diagram illustrating the Felici mechanism. The instability is caused by the action of **E** on the non-uniform distribution of space charges in the fluid, arising from unipolar charge injection from one of the electrodes.

This model has been extended to the case of DC instability in nematics by de Gennes [34]. Assuming strong injection of charges he finds that the Felici threshold is lowered by the additional space charge formation due to the conductivity anisotropy.

The threshold voltage calculated on the basis of the Felici mechanism is much higher than the experimentally observed values. Turnbull [35] has reanalyzed the DC instability in isotropic liquids by taking into account charge injection from both electrodes. This model leads to a threshold field [3]

$$E_{th} = T\ 16\ \pi^2 \eta\ \sigma / \epsilon^2 \quad ,$$

where a is the conductivity. The coefficient T depends on the ratio of mobilities of the two types of charge carriers.

As pointed out by the Orsay group [9], charge injection will be negligible at frequencies greater than 1 , t_c □ d^2 /μV being the transit time of the charge carriers across the nematic layer of thickness d. For a 20 μm thick sample of MBBA, this cut-off frequency for charge injection is about 10 Hz. However, Barnik et al. [36] have extended the model of Turnbull to much higher

frequencies. Here the non-uniform charge distribution is assumed to be caused by the electrolytic separation of the charges in the volume of the sample. In the absence of instability and for the case of a weak electric current the space charge distribution is given by

$$dQ/dz = -r\, E_z ,$$

r being the corresponding kinetic coefficient. The action of E_z on the space charges produces a destabilizing force leading to a convective flow in the medium when E_z is sufficiently large. Barnik et al. [36] obtain qualitative expressions for the threshold field based on dimensional arguments. This model indicates two regimes of instability: a low frequency regime where [3,36]

$$E_{th}^2 \propto \eta\sigma/(r\,\epsilon^2) , \qquad f << f_L$$

and a high frequency regime where

$$E_{th}^2 \propto \eta f/(r\,\epsilon) , \qquad f >> f_L$$

where $f_L = 1/2\pi\tau_L$ and $\tau_L = \epsilon/4\pi\sigma$ is the relaxation time of the space charges. Note that the anisotropies of the physical properties do not play any role in this mechanism Hence it is known as the isotropic mechanism.

Thus, according to these models, the EHD instability is caused by unipolar or bipolar charge injection at low frequencies and by the electrolytic separation of the charges at high frequencies. At frequencies much greater than the charge relaxation frequency f_L, it is clear that the instability should be confined to regions close to the electrodes. The instability patterns reported by Kai et al. in MBBA [37] may be of this origin.

Barnik et al. [36] have proposed the isotropic mechanism as an alternative explanation for the dielectric regime in nematics with $a_a > 0$. However, the experiments of Ribotta and Durand [38] clearly indicate that this mechanism is not responsible for the dielectric regime. In thick samples they were able to differentiate between the onset of an irregular convective flow and a regular flow accompanied by the appearance of an optical domain pattern. The threshold field corresponding to the irregular flow is lower and does not show any discontinuity at the NI transition point. On the other hand, the threshold field for the domain formation diverges as the NI transition point is approached (Fig.20). Ribotta and Durand attribute the irregular flow to the isotropic mechanism and the domain formation accompanied

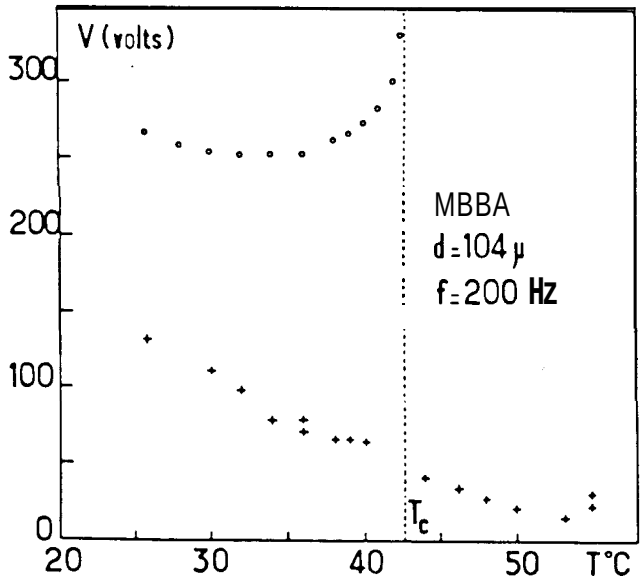

Fig.20. Variation of the threshold voltage for the pattern formation accompanied by regular cellular flow (○) and the threshold voltage for the onset of irregular flow (+) with temperature. Tc is the nematic-isotropic transition temperature. (from Ref.38).

by the regular convective flow to the Carr-Helfrich mechanism.

As mentioned earlier Blinov et al. [31] interpret the EHD instabilities in nematics with $\sigma_a < 0$ in terms of the isotropic mechanism. The observed dependence of E_{th} on σ and f are in agreement with the theory both at very low frequencies ($f << f_L$) and at very high frequencies ($f >> f_L$). Nevertheless, the theory does not predict the direction and magnitude of the wavevector of the convective rolls. Further, the qualitative nature of the theory makes a direct comparison with the experimental results impossible.

In conclusion, we emphasize that the Carr-Helfrich and the isotropic mechanisms do not offer a satisfactory explanation for the following observations:
1) Occurrence of oblique rolls upto a frequency $f_o \propto f_c$ in the conduction regime.
2) The large tilt angle of the wavevector of the convective rolls with respect to the undistorted director in the chevron pattern observed in the dielectric regime.
3) The magnitude and direction of the wavevector of the convective rolls in the EHD instability in nematics with $\sigma_a < 0$ at low frequencies ($f << f_L$).

In this thesis our main aim is to demonstrate the influence of flexoelectricity [39] on the EHD instabilities in nematics. The flexoelectric polarization arises from splay and bend distortions of the director field in a nematic and hence is characteristic of the orientational ordering in the medium. We shall therefore confine our attention to the Carr-Helfrich mechanism which is the only instability mechanism arising from the nematic ordering. The isotropic mechanism which,. as described by the Russian group, could be important in some special situations is not discussed further.

REFERENCES

1. S. Chandrasekhar, Hydrodynamic and Hydromagnetic stability, Oxford, Clarendon (1961).
2. E. Dubois-Violette, G. Durand, E. Guyon, P. Manneville and P. Pieranski, Solid state physics, supplement 14, L. Liebert ed. (1978), p 147.
3. L.M. Blinov, Electro-optical and magneto-optical properties of liquid crystals, Wiley (1983).
4. W.J.A. Goossens, Advances in liquid crystals,Vol 3, G.H. Brown ed., Academic, New York, (1978).
5. V. Freedecricksz and V.N. Tsvetkov, Phys. Z. Soviet Union, 6,490 (1934); V. Freedericksz and V. Zolina, Trans. Faraday Soc., 29, 919 (1933).
6. R. Williams, J. Chem. Phys., 39, 384 (1963).
7. G.E. Zvereva and A.P. Kapustin, Primeneniye Ul'traakustiki k Issledovaniyu Veshchestva, vol. 15, Moskovsk. Oblastnoi Pedagogich Inst., Moscow, 1961, p 69.
8. G.H. Heilmeier, L.A. Zanoni and L.A. Barton, Proc. IEEE, 56, 1162 (1968); A.P. Kapustin and L.K. Vistin, Kristallografiya, 10, 118 (1965); G. Elliot and J.G. Gibson, Nature, 205, 995 (1965).
9. Orsay liquid crystal group, Mol. Cryst. Liq. Cryst., 12, 251 (1971).
10. P.A. Penz, Mol. Crst. Liq. Cryst., 15, 141 (1971).
11. W. Helfeich, J. Chem. Phys., 51, 4092 (1969).

12. E.F. Carr, J. Chem. Phys., 39, 1979 (1963).

13. E. Dubois-Violette, P.G. de Gennes and O. Parodi, J. de Phys., 32, 305 (1971).

14. P.A. Penz and G.W. Ford, Phys. Rev A6, 414 (1972).

15. S.A. Pikin, Sov. Phys. JETP, 33, 641 (1471).

16. R.A. Kashnow and H.S. Cole, J. Appl. Phys., 42, 2134 (1971).

17. G.H. Heilmeier and W. Helfrich, Appl. Phys. Lett., 16, 1955 (1970).

18. Orsay liquid crystal group, Phys. Rev. Lett., 25, 1642 (1970).

19. I.W. Smith, Y. Galerne, S.T. Lagerwall, E. Dubois-Violette and G. Durand, J. de Phys., 36, C1- 237 (1975).

20. P. Sengupta and A. Saupe, Phys. Rev., A9,2698 (1974)

21. See for example, L. Cessari, Asymptotic behaviour and stability problems in ordinary differential equations, Academic, New York (1963).

22. C. Hilsum and F.C. Saunders, Mol. Cryst. Liq. Cryst., 64, 25 (1980).

23. S. Hirata and T. Tako, Jpn. J. Appl. Phys., 20, L459 (1981).

24. R. Ribotta, A. Joets and L. Lei, Phys. Rev. Lett., 56, 1595 (1986).

25. W. Zimmermann and L. Kramer, Phys. Rev. Lett., 55, 403 (1985).

26. V.A. Raghunathan and N.V. Madhusudana, Pramana- J. Phys., 31, L163 (1988).

27. E. Bodenschatz, W. Zimmermann and L. Kramer, J. de Phys., 49, 1875 (1988).

28. F. Rondelez, Sol. State commun., 12, 1675 (1972).

29. M. Goscianski and L. Leger, J. de Phys., 36, C1-231 (1975).

30. M. Goscianski, Philips Res. Reports, 30, 37 (1975).

31. L.M. Blinov, M.I. Barnik, V.T. Lazareva and A.N. Trufanov, J. de Phys., 40, C3-263 (1979).

32. N.J. Felici, Rev. Gen. Electr., 78, 717 (1969).

33. P. Atten and R. Moreau, C. R. Acad. Sci., 270A, 415 (1970).

34. P.G. de Gennes, Comments Sol. State Phys., 3, 35 (1970).

35. R.J. Turnbull, J. Phys. (D), 6, 1745 (1973).

36. M.I. Barnik, L.M. Blinov, S.A. Pikin and A.N. Trufanov, Sov. Phys. JETP, 45, 396 (1977)

37. S. Kai, K. Yamaguchi and K. Hirakawa, Jpn. J. Appl. Phys., 14, 1653 (1975).

38. R.Ribotta and G. Durand, J. de Phys., 40, C3-334 (1979).

39. R.B. Meyer, Phys. Rev. Lett., 22, 918 (1969).